Adiabatic Nuclear and Electronic Sampling Monte Carlo Simulations in the Gibbs Ensemble: Application to Polarizable Force Fields for Water

Bin Chen, Jeffrey J. Potoff, and J. Ilja Siepmann*

Department of Chemistry and of Chemical Engineering and Materials Science, University of Minnesota, 207 Pleasant Street SE, Minneapolis, Minnesota 55455-0431

Received: July 19, 1999; In Final Form: December 13, 1999

The adiabatic nuclear and electronic sampling Monte Carlo algorithm (ANES-MC) is extended to simulations in the Gibbs ensemble. Whereas the maximum displacements used for translational, rotational, and volume trial moves can be adjusted to foster efficient sampling in the adiabatic limit, the transfer (swap) of particles always causes a major disturbance of the electronic structures of the two phases (supplying and receiving the particle). To reequilibrate the electronic structures requires additional sampling of the electronic degrees of freedom. A simple, distance-dependent criterion for the preferential selection of the electronic degrees of freedom, for which a move is to be attempted, is shown to improve the efficiency of the particle swap move. The ANES-MC algorithm is applied to the polarizable simple point charge-fluctuating charge (SPC−FQ) and transferable intermolecular potential 4 point-fluctuating charge (TIP4P−FQ) models proposed by Rick et al. (*J. Chem. Phys*. **1994**, *101*, 6141). For both models simulations were performed using the standard constraint on the neutrality of individual molecules. In addition, for the SPC−FQ model the use of a constraint on the neutrality of an entire phase was investigated, which allows for intermolecular charge transfer. Simulations in the Gibbs ensemble were performed to calculate the vapor−liquid coexistence curves from 323 to 523 K, whereas simulations in the grand canonical ensemble were performed for the near-critical region. Dielectric constants at different state points were calculated from canonical ensemble simulations. Neither the SPC−FQ nor the TIP4P−FQ force fields give a satisfactory description of the vapor−liquid equilibria. In particular, the critical temperature is greatly underestimated by both models. Although intermolecular charge transfer has only a very small influence on the internal energy and the radial distribution functions at ambient conditions and along the coexistence curve, it increases the dielectric constant by approximately 30%.

1. Introduction

Water's unusual properties and unique importance for life and technology have lead to a plethora of theoretical and molecular modeling research on the behavior of water. However, water's properties are the result of a unique combination of intermolecular forces, such as small size, high charge density, and the ability to act as acceptor for two hydrogen bonds and donor for another two hydrogen bonds. The high charge density and the hydrogen-bonding ability cause large changes in the electronic structure of a water molecule in response to its environment. Thus a water force field, which is supposed to work under different physical conditions, requires the explicit modeling of changes in the electronic structure. Examples can be found in the many empirical polarizable water models that mimick changes in the electronic structure via polarizable dipoles or fluctuating partial charges,[1−7] and in the ab initio water models that include a direct modeling of the electronic structure using molecular orbitals or plane waves.[8−10] Including any treatment of electronic structure, however, adds to the complexity of the simulated system and thus requires more computer resources. In addition, with particular respect to the prediction of thermophysical properties, such as vapor−liquid coexistence curves, the performance of the empirical-derived polarizable models has been disappointing.[11] For these reasons, the common nonpolarizable water models, like SPC,[12] SPC/E,[13] and TIP4P,[14] remain the popular choice of the simulation community for most applications.[15]

The position of chemical and phase equilibria and the direction of all spontaneous chemical change are determined by free energies. Whereas the determination of mechanical properties is now routine for computer simulation, the determination of thermal properties and phase equilibria, which depend on the volume of phase space, remains one of the most challenging problems.[16] For calculations of thermal properties and phase equilibria, the Monte Carlo method offers substantial advantages over the molecular dynamics technique.[17] In particular, Gibbs ensemble Monte Carlo (GEMC)[18−20] has become the leading technique for the determination of vapor−liquid and liquid−liquid equilibria. Simulations in the Gibbs ensemble involve at least two phases that are treated using separate, but thermodynamically connected simulation boxes. In addition to the usual translations, rotations, and conformational changes of molecules, simulations in the Gibbs ensemble use particle swaps between the boxes to achieve phase equilibrium (equal chemical potential for a given species in all phases) and volume moves to achieve mechanical equilibrium (equal pressure in all phases).

The first Gibbs ensemble simulations for water were performed by de Pablo et al.,[21] who obtained the vapor−liquid phase diagram for the SPC model. These simulations showed that the SPC model greatly underpredicts the critical temperature and density, while the saturated vapor pressures at low temperatures are relatively well described. Strauch and Cummings[22]

* Corresponding author. E-mail: siepmann@chem.umn.edu.

10.1021/jp992459p CCC: $19.00
Published on Web 02/23/2000

proposed a modification to the SPC model that involved reducing the magnitude of the partial charges in *only* the gas phase by a factor of $(1.8/2.24)^{1/2}$. Use of this modified SPC model considerably improved the predicted vapor−liquid equilibria, thus pointing to the importance of accounting for water's change in electronic structures between the vapor and liquid environment.

Mederios and Costas[23] attempted the first calculation to determine the vapor−liquid phase envelope for a polarizable force field using a pseudo-Gibbs ensemble technique in which the gas phase is not modeled explicitly, but approximated using a virial equation of state which limits the calculation to low temperatures. A matrix inversion technique was utilized to optimize the partial charges of *only* the trial molecule. (A full minimization of the electronic structure was deemed too expensive.) Medeiros and Costas reported that the total energy obtained by this approximation differs from that calculated by a full optimization of all partial charges by 0.5% [O (10^4 K) for their water systems at 298 K]. The calculations of Medeiros and Costas show that the coexistence curve of the TIP4P−FQ model[5] deviates significantly from the experimental results for temperatures as low as 373 K. Kiyohara et al.[11] investigated the vapor−liquid equilibria for several dipole-polarizable water force fields through grand canonical Monte Carlo simulations. Unfortunately, they found that none of the polarizable models studied was able to give satisfactory results for the near-critical region of the phase diagram. Kiyohara et al. used an iterative procedure to minimize the electronic energy during every Monte Carlo move, which was necessary to achieve the required adiabatic separation of nuclear and electronic degrees of freedom. Use of an iterative procedure has two major disadvantages. First, a very high accuracy of the iterative scheme (large number of iterations) is needed to sample from an ensemble distribution that corresponds to the correct Born−Oppenheimer (BO) limit. Second, the fact that the electronic structure must be optimized at every move results in a computational cost that scales as N^3 (where N is the number of particles) instead of the N^2 scaling found for nonpolarizable models. Recently, Yezdimer and Cummings[24] performed additional calculations for the vapor−liquid coexistence curve of the TIP4P−FQ water model. The Gibbs−Duhem integration technique[25] was used, and molecular dynamics simulations of the liquid and vapor phases were performed separately in the isobaric−isothermal ensemble to calculate the difference in molar enthalpy and molar volume between these two phases. The coexistence point obtained by Medeiros and Costas[23] at 298 K was chosen as the initial condition for the integration. Yezdimer and Cummings concluded that the TIP4P−FQ model does not predict the coexistence curve of water well compared with other simpler nonpolarizable models.

Previously, we proposed a novel Monte Carlo algorithm, called adiabatic nuclear and electronic sampling Monte Carlo (ANES-MC), for simulations of polarizable force fields in the canonical ensemble.[26,27] In ANES-MC, the electronic degrees of freedom are treated as classical degrees of freedom subject to a secondary low-temperature thermostat in close analogy to the extended Lagrangian formalism used in molecular dynamics simulations.[1,28−31] As in Car−Parrinello molecular dynamics,[29] the electronic degrees of freedom are optimized "on-the-fly" during every nuclear move in ANES-MC. Using the new algorithm, the cost of canonical-ensemble Monte Carlo simulations using fluctuating-charge force fields increases by less than an order of magnitude compared with simulations using the parent fixed-charge force fields.

In this article, we extend the ANES-MC algorithm to simulations in the Gibbs ensemble. In particular, we introduce volume and particle swap moves using the ANES-MC scheme. We will show that an efficient particle swap move requires an additional preferential selection of the electronic degrees of freedom on which trial displacements are attempted during the electronic move sequence (EMseq) of the ANES-MC algorithm. The combination of ANES-MC and GEMC was used to obtain the vapor−liquid coexistence curves for the polarizable SPC−FQ and TIP4P−FQ models.[5] In addition, it is shown that the computational cost of an ANES-MC calculation in the canonical and Gibbs ensembles scales as N^2.

The remainder of this article is arranged as follows. The next section gives a detailed description of the simulation algorithms used in this work and briefly discusses the molecular models studied. Numerical results for the vapor−liquid coexistence curves, structural properties, and dielectric constants are presented in section 3.

2. Simulation Methodology and Models

A. Matrix Minimization Monte Carlo Algorithm. The matrix minimization Monte Carlo (MM-MC) algorithm was introduced by us to test the validity of the ANES-MC scheme for simulations of polarizable systems in the canonical ensemble. It can be straightforwardly extended to the Gibbs ensemble. Given a set of nuclear coordinates, the MM-MC algorithm uses the method of Lagrange undetermined multipliers to minimize an electronic energy functional given in the form of a matrix equation.[27] Thus any configuration visited by the MM-MC method corresponds to its electronic ground state, the Born−Oppenheimer (BO) limit, and the potential energy of the system is a function of *only* its nuclear coordinates. For a one-component system, the constant-volume Gibbs ensemble partition function of such a system that is always in its electronic ground state is identical with the partition function for a nonpolarizable system, and can be written as follows[20]:

$$Q(N,V,T) = \frac{1}{\Lambda^{3N}} \sum_{V_1=0}^{V} \sum_{N_1=0}^{N} \frac{V_1^{N_1} (V - V_1)^{N-N_1}}{N_1!(N - N_1)!} \times \int_{V_1} \exp[-\beta U_1(\mathbf{s}_1, V_1)] d\mathbf{s}_1 \times \int_{V-V_1} \exp[-\beta U_2(\mathbf{s}_2, V - V_1)] d\mathbf{s}_2 \quad (1)$$

where N, N_1, V, and V_1 are the total number of molecules in the combined system, the number of molecules in box 1, the total volume, and the volume of box 1, respectively. The variable T is the absolute temperature, and $\beta = (k_B T)^{-1}$ is the inverse temperature where k_B is Boltzmann's constant. Λ is the de Broglie thermal wavelength. The potential energy U_x of box x is specified by the set of reduced coordinates $\boldsymbol{s}$ of all particles in the box and the volume of the box.

Starting from a given nuclear and ground-state electronic configuration, the MM-MC algorithm proceeds as follows:

(i) Attempt any type of displacement of nuclear coordinates (translation, rotation, volume exchange, or particle swap).

(ii) Find the electronic ground state for the nuclear trial configuration by the matrix minimization process.

(iii) Accept/reject the nuclear move using the standard Gibbs ensemble acceptance rules for the different types of moves.[18−20]

B. Adiabatic Nuclear and Electronic Sampling Monte Carlo Algorithm. In adiabatic sampling schemes using a finite electronic temperature (T_{elec}), the electronic configuration is

treated as a set of classical degrees of freedom, and there is a continuous distribution of electronic states (defined by a set of electronic coordinates **q**) for every nuclear configuration. Thus the electronic degrees of freedom have to be included explicitly in the partition function.[27] For quadratic coupling of the electronic degrees of freedom which leads to an electronic phase volume that is independent of the nuclear coordinates (and a set of normal electronic coordinates **p** that is independent of **s**), we previously demonstrated that the canonical partition function of a system with nuclear and electronic degrees of freedom can be separated into its nuclear and electronic parts as follows[27,32]:

$$Q_{ne}(N, V, T, T_{elec}) = Q_{nucl}(N, V, T) \times Q_{elec}(N, T'_{elec}) \quad (2a)$$

$$Q_{nucl}(N, V, T) = \frac{V^N}{\Lambda^{3N} N!} \int \exp[-\beta E_{gs}(\mathbf{s}, V)]\, d\mathbf{s} \quad (2b)$$

$$Q_{elec}(N, T'_{elec}) = \frac{1}{\Lambda_{elec}^{cN}} \int \exp[-\beta' \epsilon(\mathbf{p})]\, d\mathbf{p} \quad (2c)$$

where $(T'_{elec})^{-1} = T^{-1} + (T_{elec})^{-1}$ and $\beta' = (k_B T'_{elec})^{-1}$. Λ and Λ_{elec} are the de Broglie thermal wavelength for the nuclear motion at temperature T and the electronic motion at T'_{elec}, respectively. c denotes the number of electronic degrees of freedom per molecule. $E_{gs}(\mathbf{s}, V)$ is the ground-state potential energy corresponding to the BO limit that depends only on the set of nuclear coordinates. The electronic energy $\epsilon(\mathbf{p})$ is the difference between the total potential energy $U(\mathbf{s}, V, \mathbf{p})$ and $E_{gs}(\mathbf{s}, V)$ and depends only on the set of normal electronic coordinates. Following this, the constant-volume Gibbs−ensemble partition function of a system with nuclear and electronic degrees of freedom can be written as:

$$\begin{aligned} Q_{ne}(N, V, T, T_{elec}) &= Q(N, V, T) \times Q_{elec}(N, T'_{elec}) \\ &= \frac{1}{\Lambda^{3N}} \frac{1}{\Lambda_{elec}^{cN}} \sum_{V_1=0}^{V} \sum_{N_1=0}^{N} \frac{V_1^{N_1} (V - V_1)^{N-N_1}}{N_1!(N - N_1)!} \\ &\times \int_{V_1} \exp[-\beta E_{gs}(\mathbf{s}_1, V_1)] d\mathbf{s}_1 \\ &\times \int_{V-V_1} \exp[-\beta E_{gs}(\mathbf{s}_2, V - V_1)] d\mathbf{s}_2 \\ &\times \int \exp[-\beta' \epsilon(\mathbf{p}_1)]\, d\mathbf{p}_1 \\ &\times \int \exp[-\beta' \epsilon(\mathbf{p}_2)]\, d\mathbf{p}_2 \end{aligned} \quad (3)$$

Starting from a given nuclear and electronic configuration, the ANES-MC algorithm in the Gibbs ensemble proceeds as follows:

(i) Attempt any type of displacement of nuclear coordinates (translation, rotation, volume exchange, or particle swap).

(ii) Perform a suitable number R_{elec} of electronic moves to sample from equilibrium electronic configurations (see section 2.C). These moves are conditionally accepted using the Metropolis acceptance criterion with temperature T_{elec}.

(iii) Accept/reject the combined nuclear/electronic move sequence (steps 1 and 2) using the standard Gibbs ensemble acceptance rules with temperature T. If rejected, return to the old nuclear *and* electronic configurations.

For translational and rotational moves that attempt changes of the nuclear and electronic configurations in *only* one of the boxes, e.g. box 1, of the Gibbs ensemble system, the acceptance rule in step iii between the old state Γ_a and the trial state Γ_b is

$$\mathrm{acc}(\Gamma_a \rightarrow \Gamma_b) = \min\left\{1, \exp\left[-\frac{U(\mathbf{s}_{1,b}, \mathbf{q}_{1,b}) - U(\mathbf{s}_{1,a}, \mathbf{q}_{1,a})}{k_B T}\right]\right\} \quad (4)$$

The corresponding super-detailed balance condition between these two states is given by

$$\begin{aligned} &\rho(\mathbf{s}_{1,a}, \mathbf{s}_2, \mathbf{q}_{1,a}, \mathbf{q}_2, N, N_1, V, V_1, T, T_{elec}) \times \\ &\qquad \alpha(\mathbf{s}_{1,b}, \mathbf{q}_{1,b}) \times \mathrm{acc}(\Gamma_a \rightarrow \Gamma_b) \\ &= \rho(\mathbf{s}_{1,b}, \mathbf{s}_2, \mathbf{q}_{1,b}, \mathbf{q}_2, N, N_1, V, V_1, T, T_{elec}) \times \\ &\qquad \alpha(\mathbf{s}_{1,a}, \mathbf{q}_{1,a}) \times \mathrm{acc}(\Gamma_b \rightarrow \Gamma_a) \end{aligned} \quad (5)$$

where ρ is the probability density obtained from eq 3,

$$\begin{aligned} &\rho(\mathbf{s}_1, \mathbf{s}_2, \mathbf{q}_1, \mathbf{q}_2, N, N_1, V, V_1, T, T_{elec}) = \\ &\qquad \rho(\mathbf{s}_1, \mathbf{s}_2, \mathbf{p}_1, \mathbf{p}_2, N, N_1, V, V_1, T, T_{elec}) \\ &= Q_{ne}(N, V, T, T_{elec})^{-1} \\ &\times \frac{1}{\Lambda^{3N}} \frac{1}{\Lambda_{elec}^{cN}} \times \frac{V_1^{N_1} (V - V_1)^{N-N_1}}{N_1!(N - N_1)!} \\ &\times \exp[-\beta E_{gs}(\mathbf{s}_1, V_1)] \times \exp[-\beta E_{gs}(\mathbf{s}_2, V - V_1)] \\ &\times \exp[-\beta' \epsilon(\mathbf{p}_1)] \times \exp[-\beta' \epsilon(\mathbf{p}_2)] \end{aligned} \quad (6)$$

and α is the nonsymmetric underlying matrix of the Markov chain.[27] This underlying matrix reflects that the probability of generating a specific electronic configuration does depend on its electronic energy because of the sampling of electronic moves in step ii. If electronic equilibrium is achieved, then the underlying matrix is given by

$$\alpha(\mathbf{s}, \mathbf{q}) = \frac{\exp[-\beta_{elec} \epsilon(\mathbf{s}, \mathbf{q})]}{\int \exp[-\beta_{elec} \epsilon(\mathbf{s}, \mathbf{q})]\, d\mathbf{q}} = \frac{\exp[-\beta_{elec} \epsilon(\mathbf{p})]}{\int \exp[-\beta_{elec} \epsilon(\mathbf{p})]\, d\mathbf{p}} \quad (7)$$

where the second equality holds because of the linear transformation between **q** and **p**, and $\beta_{elec} = (k_B T_{elec})^{-1}$. Reorganization of eq 5 yields

$$\begin{aligned} &\frac{\rho(\mathbf{s}_{1,a}, \mathbf{s}_2, \mathbf{q}_{1,a}, \mathbf{q}_2, N, N_1, V, V_1, T, T_{elec})}{\rho(\mathbf{s}_{1,b}, \mathbf{s}_2, \mathbf{q}_{1,b}, \mathbf{q}_2, N, N_1, V, V_1, T, T_{elec})} = \\ &\qquad \frac{\alpha(\mathbf{s}_{1,a}, \mathbf{q}_{1,a}) \times \mathrm{acc}(\Gamma_b \rightarrow \Gamma_a)}{\alpha(\mathbf{s}_{1,b}, \mathbf{q}_{1,b}) \times \mathrm{acc}(\Gamma_a \rightarrow \Gamma_b)} \end{aligned} \quad (8)$$

Inserting eqs 4, 6, and 7 into eq 8 and recognizing that the terms in V^N, $\mathbf{N}!$, Λ^N, and Q_{ne} cancel yields (where we have dropped the V descriptor after the scaled coordinates because the volume is constant)

$$\frac{\exp[-\beta E_{gs}(\mathbf{s}_{1,a})]\exp[-\beta E_{gs}(\mathbf{s}_2)]\exp[-\beta'\epsilon(\mathbf{p}_{1,a})]\exp[-\beta'\epsilon(\mathbf{p}_2)]}{\exp[-\beta E_{gs}(\mathbf{s}_{1,b})]\exp[-\beta E_{gs}(\mathbf{s}_2)]\exp[-\beta'\epsilon(\mathbf{p}_{1,b})]\exp[-\beta'\epsilon(\mathbf{p}_2)]} = \frac{\exp[-\beta_{elec}\epsilon(\mathbf{p}_{1,b})]/\int \exp[-\beta_{elec}\epsilon(\mathbf{p}_1)]\,d\mathbf{p}_1}{\exp[-\beta_{elec}\epsilon(\mathbf{p}_{1,a})]/\int \exp[-\beta_{elec}\epsilon(\mathbf{p}_1)]\,d\mathbf{p}_1} \times \frac{\exp[-\beta(E_{gs}(\mathbf{s}_{1,a})] + \epsilon(\mathbf{p}_{1,a}))}{\exp[-\beta(E_{gs}(\mathbf{s}_{1,b})] + \epsilon(\mathbf{p}_{1,b}))} \quad (9a)$$

$$\frac{\exp[-\beta E_{gs}(\mathbf{s}_{1,a})]\exp[-\beta'\epsilon(\mathbf{p}_{1,a})]}{\exp[-\beta E_{gs}(\mathbf{s}_{1,b})]\exp[-\beta'\epsilon(\mathbf{p}_{1,b})]} = \frac{\exp[-\beta_{elec}\epsilon(\mathbf{p}_{1,b})]}{\exp[-\beta_{elec}\epsilon(\mathbf{p}_{1,a})]} \times \frac{\exp[-\beta(E_{gs}(\mathbf{s}_{1,a}) + \epsilon(\mathbf{p}_{1,a}))]}{\exp[-\beta(E_{gs}(\mathbf{s}_{1,b}) + \epsilon(\mathbf{p}_{1,b}))]} \quad (9b)$$

From the definition of T'_{elec} it follows that all Boltzmann weights depending on the electronic energies cancel, and the detailed balance equality is satisfied. Thus sampling from the Gibbs ensemble distribution in the BO limit is achieved.

In an analogous way, it can be demonstrated that the acceptance rule for volume moves using displacement uniform in $\log(V)$ is given by

$$\mathrm{acc}(\Gamma_a \rightarrow \Gamma_b) = \min\left\{1, \left(\frac{(V_1)^{N_1+1}(V-V_1)^{N-N_1+1}}{(V_1+\Delta V)^{N_1+1}(V-V_1-\Delta V)^{N-N_1+1}} \exp\left[-\frac{U(\mathbf{s}_{1,b}, V_1, \mathbf{q}_{1,b}) - U(\mathbf{s}_{1,a}, V_1+\Delta V, \mathbf{q}_{1,a})}{k_B T}\right] \exp\left[-\frac{U(\mathbf{s}_{2,b}, V-V_1, \mathbf{q}_{2,b}) - U(\mathbf{s}_{2,a}, V-V_1-\Delta V, \mathbf{q}_{2,a})}{k_B T}\right]\right)\right\} \quad (10)$$

and for particle swap moves (from box 1 to box 2) one obtains

$$\mathrm{acc}(\Gamma_a \rightarrow \Gamma_b) = \min\left\{1, \left(\frac{(V-V_1)N_1}{V_1(N-N_1+1)} \exp\left[-\frac{U(\mathbf{s}_{1,b}, V_1, \mathbf{q}_{1,b}) - U(\mathbf{s}_{1,a}, V_1, \mathbf{q}_{1,a})}{k_B T}\right] \exp\left[-\frac{U(\mathbf{s}_{2,b}, V-V_1, \mathbf{q}_{2,b}) - U(\mathbf{s}_{2,a}, V-V_1, \mathbf{q}_{2,a})}{k_B T}\right]\right)\right\} \quad (11)$$

C. Details of the Electronic Move Sequences during ANES-MC. An electronic move involves the displacement of a *set* of randomly selected electronic coordinates obeying any imposed neutrality constraint, that is either neutrality of any given molecule or neutrality of the entire phase. In the former case, an electronic move for a randomly selected molecule with n fluctuating partial charges involves the random selection of one partial charge which is then changed by an amount of dq selected uniformly from the range $(-d_{elec}; +d_{elec})$ (where d_{elec} is the maximum charge displacement). To impose the neutrality of the trial molecule, there are two obvious options: (i) change the charges of the other $n-1$ sites by $-dq/(n-1)$ or (ii) pick a second charge site on the same molecule at random and change its charge by $-dq$. The first option is used in our work on three-charge-site water models. If the neutrality constraint acts on the entire phase (thereby allowing intermolecular charge transfer), the electronic move involves the random selection of two charge sites, which may or may not belong to the same molecule. One of these two charges is displaced by an amount dq selected uniformly from the range $(-d_{elec}; +d_{elec})$, whereas the other is changed by $-dq$. Spreading the displaced charge over the entire phase [$(N \times n) - 1$ charge sites] is clearly not efficient, because it would entail a calculation of the electronic energy of the entire phase. The acceptance rules described in the previous section require that an equilibrium electronic configuration is reached during the electronic move sequence (EMseq). The computational cost of the ANES-MC algorithm, however, depends directly on the number of electronic moves performed during the EMseq (step 2). For sampling in the canonical ensemble, we have previously demonstrated that the overall efficiency of the ANES-MC algorithm can be greatly improved by a judicious choice of maximum translational and rotational displacements (d_{trans} and d_{rot}) that allows the system to move within the BO skin created by the finite electronic temperature. In ref 27, we suggested monitoring the energy evolution during the EMseq. The convergence of the total energy was used as a criterion for the selection of maximum displacements and R_{elec}.

Here we advocate an additional test for the performance of the EMseq. During short test calculations we use the matrix minimization method to calculate E_{gs} for every nuclear trial configuration. Knowing E_{gs} allows us to obtain the value of ϵ (the electronic energy) at any time during the simulation ($\epsilon = U - E_{gs}$). Now the distribution of ϵ can be calculated for the last configuration sampled in all EMseq and for all configurations included in the ensemble averages. In principle, these two distributions should differ because the EMseq samples the electronic degrees of freedom at T_{elec}, whereas the ensemble average should be characterized by T'_{elec}. However, the standard choice of $T = 298$ K and $T_{elec} = 5$ K yields $T'_{elec} = 4.92$ K, a difference of less than 2%. Figure 1 shows comparisons of the ensemble-averaged ϵ distributions for different combinations of maximum displacements, numbers of electronic moves, and electronic temperatures obtained from canonical ensemble simulations of 100 SPC−FQ water molecules (see section 2.D for a description of the force field) at $T = 298$ K and $\rho = 1.0$ g/mL. With a constraint on the neutrality of the molecule, there are two electronic degrees of freedom per water molecule. It should be noted that the x-axis scales are adjusted to reflect the range of observed ϵ values for the different conditions. Using $d_{trans} = 0.3$ Å and $d_{rot} = 0.4$ rad for the maximum translational and rotational displacements results in acceptance rates of approximately 45% for these two types of moves, whereas the sets of intermediate maximum displacements (0.1 Å and 0.1 rad) and smallest displacements (0.05 Å and 0.05 rad) yield acceptance rates close to 80% and 90%, respectively. The most important observation is that the number of electronic moves, R_{elec}, that yields an electronic energy distribution close to the distribution obtained for 200 uncoupled harmonic oscillators (the equilibrium distribution for full adiabatic separation), depends strongly on the set of maximum displacements. Although $R_{elec} = 50$ is sufficient for the smallest displacements used here, 100 or 1000 electronic moves are needed for the intermediate and large sets of maximum displacements. In addition, fewer electronic moves are required in simulations using a higher electronic temperature to achieve sampling from the equilibrium distribution. However, it is important to note that use of $R_{elec} = 1$ (which leads to the smallest increase in computational cost) yields an ϵ distribution that is shifted to significantly higher energies than that expected for full adiabatic separation. A special case for the ANES-MC algorithm is obtained by selecting $T_{elec} = \infty$ K, for which *all*

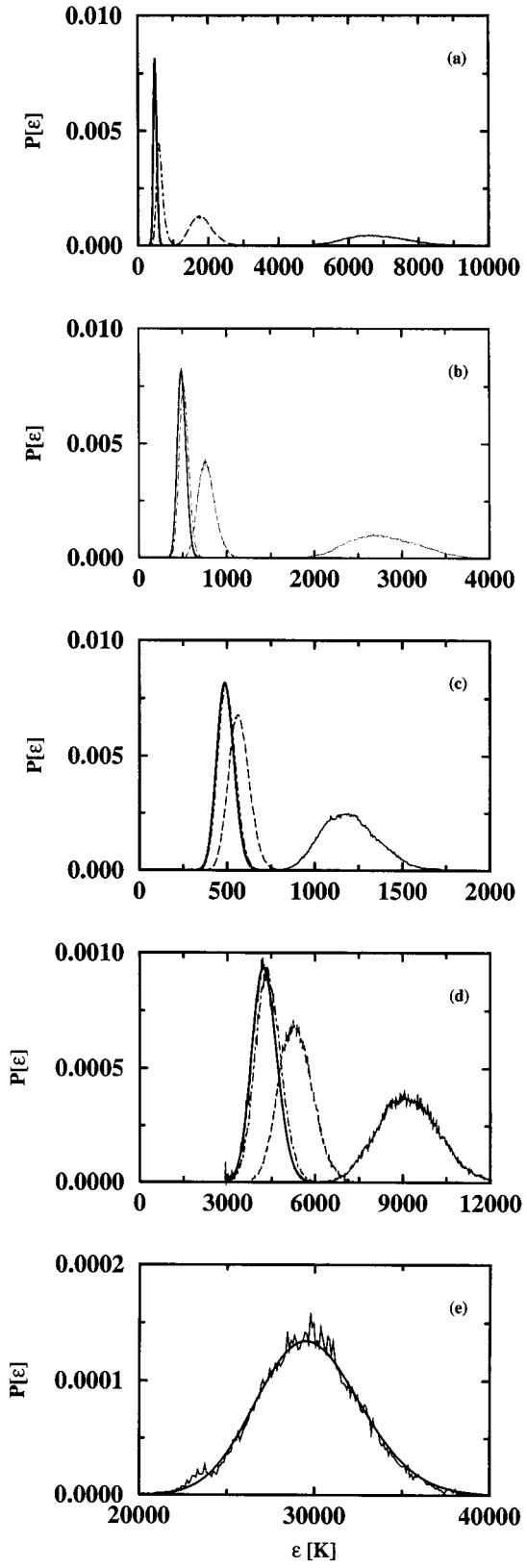

Figure 1. Translational and rotational moves: Distributions of the electronic energy (ϵ) obtained from the ensemble average using (a) $T_{elec} = 5$ K ($T'_{elec} = 4.92$ K), $d_{trans} = 0.3$ Å, and $d_{rot} = 0.4$ rad; (b) $T_{elec} = 5$ K, $d_{trans} = 0.1$ Å, and $d_{rot} = 0.1$ rad; (c) $T_{elec} = 5$ K, $d_{trans} = 0.05$ Å, and $d_{rot} = 0.05$ rad; (d) $T_{elec} = 50$ K ($T'_{elec} = 42.8$ K), $d_{trans} = 0.3$ Å, and $d_{rot} = 0.4$ rad; and (e) $T_{elec} = \infty$ K ($T'_{elec} = 298$ K), $d_{trans} = 0.3$ Å and $d_{rot} = 0.4$ rad. The thick lines represent the distributions calculated for 200 uncoupled harmonic oscillators at T'_{elec}. The solid, dashed, dot−dashed, and dotted lines represent simulations using $R_{elec} = 1$, 10, 100, and 1000, respectively.

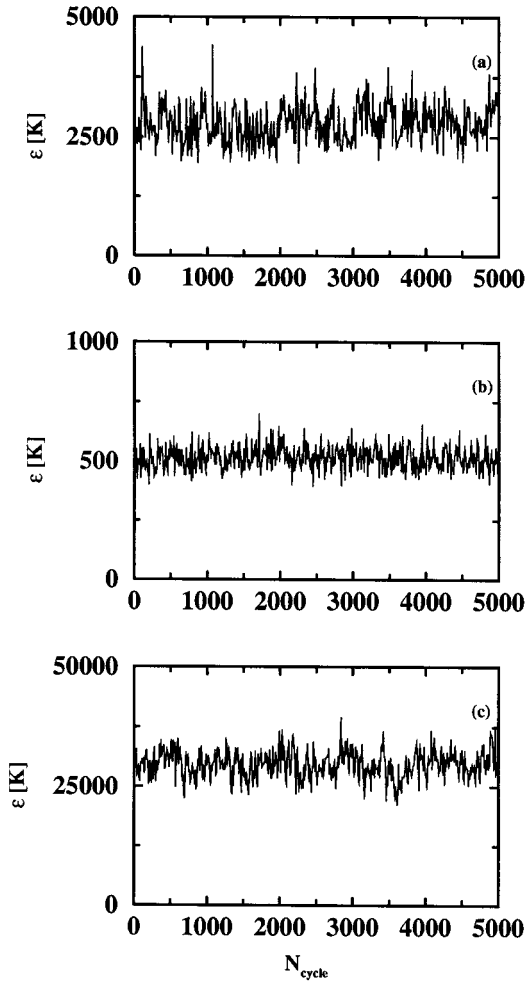

Figure 2. Translational and rotational moves: Instantaneous values of the electronic energy (ϵ) starting from an equilibrated (nuclear and electronic) configuration using (a) $T_{elec} = 5$ K and $R_{elec} = 1$; (b) $T_{elec} = 5$ K and $R_{elec} = 100$; and (c) $T_{elec} = \infty$ K ($T'_{elec} = 298$ K) and $R_{elec} = 1$. The maximum displacements were $d_{trans} = 0.1$ Å and $d_{rot} = 0.1$ rad.

electronic moves in step ii are accepted and which leads to $T'_{elec} = T = 298$ K (i.e. the nuclear and electronic degrees of freedom are sampled using the same temperature). In this case, one might also allow electronic moves as regular moves in the ANES-MC algorithm, which then becomes formally identical with the sequential fluctuating charge Monte Carlo (SFQ-MC) algorithm introduced previously.[26,27] Because both nuclear and electronic degrees of freedom are sampled using the same temperature, any set of maximum displacements will work here.

As mentioned above, selecting $R_{elec} = 1$ is computationally efficient, but might not yield sampling of the nuclear degrees of freedom from distribution described by eq 3 because the electronic degrees of freedom have a too high energy and are therefore not sampled according to eq 2. The offset in electronic energy is caused by the electronic motion lagging behind the nuclear motion during step ii with $R_{elec} = 1$. In this case, it is important to test whether the electronic energy will reach a steady state or will diverge over the course of the simulations. In Figure 2, instantaneous values of the electronic energy are plotted as function of the length of the simulation. It is clearly evident that a steady state is reached even for $R_{elec} = 1$. However, although the electronic energies fluctuate around the expected values for $R_{elec} = 100$ and $T_{elec} = 5$ K ($\langle\epsilon\rangle/k_B = 515 \simeq 100 \times T'_{elec} = 492$ K) and $R_{elec} = 100$ and $T_{elec} = \infty$ K ($\langle\epsilon\rangle/k_B = 29\,700$ K $\simeq 100 \times T'_{elec} = 29\,800$ K), this is

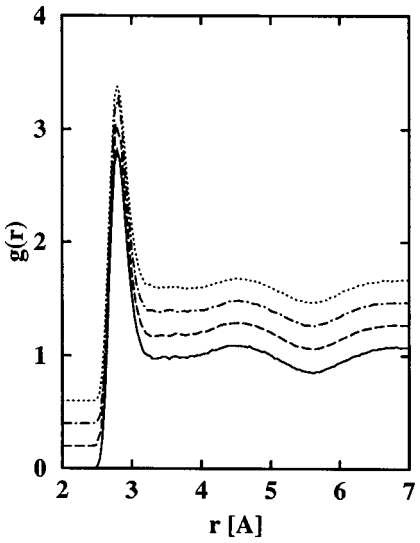

Figure 3. Oxygen−oxygen radial distribution functions obtained for SPC−FQ water ($T = 298$ K, $\rho = 1.0$ g/mL) using MM-MC with $N = 100$, $d_{trans} = 0.3$ Å and $d_{rot} = 0.4$ rad (solid line), ANES-MC with $N = 100$, $d_{trans} = 0.1$ Å, $d_{rot} = 0.1$ rad, $T_{elec} = 5$ K, and $R_{elec} = 1$ (dashed line, vertically offset by 0.2 units); ANES-MC with $N = 500$, $d_{trans} = 0.1$ Å, $d_{rot} = 0.1$ rad, $T_{elec} = 5$ K, and $R_{elec} = 1$ (dashed−dotted line, vertically offset by 0.4 unit); and ANES-MC with $N = 100$, $d_{trans} = 0.3$ Å, $d_{rot} = 0.4$ rad, $T_{elec} = \infty$ K, and $R_{elec} = 1$ (dotted line, vertically offset by 0.6 unit).

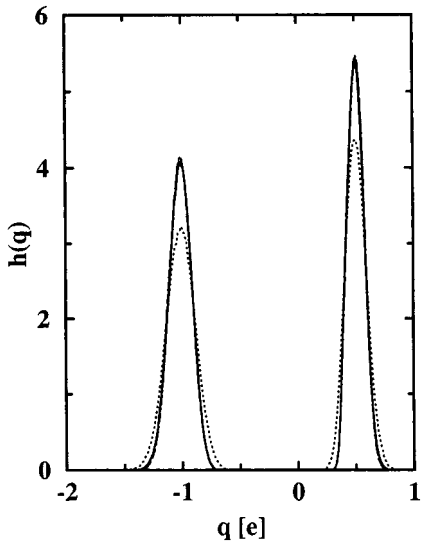

Figure 4. Oxygen and hydrogen charge distributions obtained for SPC−FQ water ($T = 298$ K, $\rho = 1.0$ g/mL). Simulation details and linestyles (without vertical offsets) are the same as in Figure 3.

obviously not the case for $R_{elec} = 1$ and $T_{elec} = 5$ K ($\langle\epsilon\rangle/k_B = 2800$ K $\neq 100 \times T'_{elec} = 492$ K).

To ascertain the influence of the different choices of T_{elec} and R_{elec} on the sampling of the nuclear degrees of freedom, we compare radial distribution functions (RDFs), which depend only on nuclear coordinates. From the oxygen−oxygen RDFs shown in Figure 3, it is evident that ANES-MC simulations with $T_{elec} = 5$ K and $R_{elec} = 1$ or with $T_{elec} = \infty$ K result in nuclear properties that do not significantly differ from the BO limit (sampled in MM-MC simulations). (As demonstrated in ref 27, this is only true for quadratic coupling of the electronic degrees of freedom.) In addition, an increase in system size (from $N = 100$ to $N = 500$) does not require an increase in R_{elec} for translational and rotational moves. Nevertheless, it should always be considered that the electronic properties have to depend on T_{elec}. Oxygen and hydrogen charge distributions are plotted in Figure 4. (The charge distributions for the two hydrogen atoms are indistinguishable.) The distributions for $T_{elec} = 5$ K do not differ significantly from the distributions obtained in the BO limit, that is the heterogeneity of the liquid water environment is mainly responsible for the width of the distributions and masks the additional (but comparably small) thermal fluctuations for $T_{elec} = 5$ K. In contrast, for $T_{elec} = \infty$ K ($T'_{elec} = 298$ K) the thermal fluctuations are clearly evident and lead to peak broadening.

The choice of optimal maximum translational and rotational displacements depends on the density of the system, and larger maximum displacements can be used for lower densities.[27] Therefore, different maximum displacements can be used for the liquid and vapor phases in Gibbs ensemble simulations.

Similar to the translational and rotational moves described above, it is possible to adjust the maximum volume displacement so that a volume move causes only a minor disturbance of the electronic structure. In our implementation of the Gibbs ensemble, the volume exchanges between the two phases use displacements uniform in $\log(V)$ (see eq 10). For a system with $N = 120$ water molecules, we found that a maximum displacement of approximately 17 Å^3 works well, whereas this value can be increased to 70 Å^3 for the larger systems with $N = 500$.

The particle swap move always involves the exchange of an entire water molecule, and there is no equivalent of the maximum displacement that could be adjusted to improve the computational efficiency. The removal/insertion of a molecule from/into the liquid phase will necessarily lead to a dramatic change of the electronic structure in the vicinity of the removal/insertion site. Similarly, a dimer might form or dissociate in the vapor phase. For the liquid phase, in particular, a large number of electronic moves may be needed to reequilibrate the electronic structure. Insufficient electronic sampling may affect the equalization of the chemical potentials between the two phases and lead to incorrect coexistence densities. Monitoring the energy evolution over the EMseq again can help to determine the required number of the electronic moves. One might also expect that more frequent sampling of the electronic degrees of freedom belonging to the swapped molecule and its former and new neighboring molecules can facilitate the equilibration of the electronic structure than sampling of electronic degrees of freedom belonging to more distant molecules whose electronic environment is much less disturbed by the particle swap. Here we suggest a strategy of preferentially selecting the electronic degrees of freedom on the molecule being swapped and its neighboring molecules for electronic moves. This can be realized by adding the following (fixed) selection criterion to the underlying matrix of the Markov chain:

$$\alpha(r) = \min(1, ar^{-b}) \tag{12}$$

where $\alpha(r)$ is the probability of randomly selecting a molecule for which an electronic move will be attempted. The separation r is the center-of-mass distance between the molecule being selected (for the electronic move) and the trial or old position of the molecule being swapped. a and b are adjustable parameters to optimize the sampling efficiency. Increasing the b parameter leads to a decrease in the range of neighboring molecules being selected preferentially. The same preferential selection criterion should be applied to both phases. Some short test simulations showed that a choice of $a = 10$ Å^b and $b = 4$ works well for Gibbs ensemble simulations of water. The evolution of the total energy during the EMseq of the particle swap move is shown in Figure 5 with and without preferential

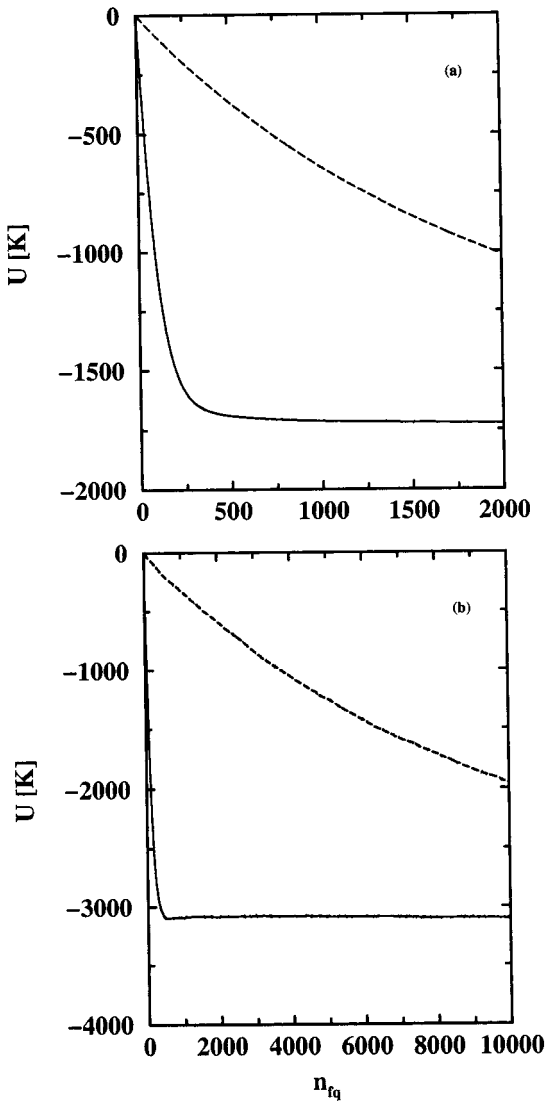

Figure 5. The mean evolution of the total energy (liquid and vapor phases) averaged over a period of 10^3 swap moves versus the number of electronic moves during the EMseq of an ANES-MC particle swap move with (solid lines) or without (dashed lines) preferential selection of the sites for the electronic move for (a) a 120-molecule system and (b) a 500-molecule system.

selection. In the latter case, 2000 electronic moves are insufficient to reequilibrate the electronic configuration for a 120-molecule simulation. In contrast, with the preferential selection strategy less than 500 electronic moves are sufficient to reequilibrate the electronic energy. The energy evolutions during the EMseq sequence for 500-molecule systems (see Figure 5) demonstrate that the preferential selection strategy is able to remove the system size dependence of the number of electronic moves that are needed during particle swap moves. For the Gibbs ensemble simulations reported in section 3, we used $R_{\text{elec}} = 1000$ for the particle swap move, where the first 500 electronic moves use the preferential selection strategy and the remaining 500 moves are carried out without bias. It is important to point out that our program performs the EMseq part for particle swap moves only if the trial position of the swapped molecule is separated from any other water molecule (oxygen−oxygen distance) by more than 1.4 Å, and if the initial trial energy is less than 100 $k_B T$. If any of these two conditions is violated, the particle swap trial is terminated immediately. Because the fraction of attempted particle swap move (over all different types of moves, that is translation, rotation, volume exchange, or particle swap) is relatively small (e.g., 0.1 for $T = 373$ K and 0.01 for $T = 473$ K) and because a large fraction of swap moves are terminated before the EMseq is started, the overall increase in computational cost of Gibbs ensemble simulations using a polarizable force field is modest (less than an order of magnitude) over the cost of simulations for the parent fixed-charge force field.

D. Models. The details of the SPC−FQ and TIP4P water models proposed by Berne and co-workers[5] can be found in the literature. Both models have the same internal geometry as their parent SPC[12] and TIP4P[14] models and use three fluctuating charges located on the hydrogen atomic sites and on or near the oxygen atomic site, and one Lennard−Jones site on the oxygen. The total energy of a water system using periodic boundary conditions and the Ewald sum with tin foil boundary conditions is given by

$$\begin{aligned} E_{\text{total}} = & \sum_{i=1}^{N-1}\sum_{j=i+1}^{N} 4\epsilon_{\text{OO}}\left[\left(\frac{\sigma_{\text{OO}}}{r_{\text{iO},j\text{O}}}\right)^{12} - \left(\frac{\sigma_{\text{OO}}}{r_{\text{iO},j\text{O}}}\right)^{6}\right] c(r_{\text{iO},j\text{O}}) + \\ & E_{\text{tail-LJ}} + \sum_{i=1}^{N-1}\sum_{j=i+1}^{N}\sum_{a=1}^{3}\sum_{b=1}^{3} q_{ia}q_{jb}\frac{\text{erfc}(\kappa r_{ia,jb})}{4\pi\epsilon_0 r_{ia,jb}} \\ & + \frac{1}{2V\epsilon_0}\sum_{k\neq 0}^{K_{\max}}\frac{\exp(-k^2/4\kappa^2)}{k^2}\left|\sum_{i=1}^{N}\sum_{a=1}^{3} q_{ia}\exp(-i\mathbf{k}\cdot\mathbf{r}_{ia})\right|^2 \\ & - \frac{\kappa}{4\pi^{3/2}\epsilon_0}\sum_{i=1}^{N}\sum_{a=1}^{3} q_{ia}^2 - \sum_{i=1}^{N}\sum_{a=1}^{2}\sum_{b=a+1}^{3} q_{ia}q_{ib}\frac{\text{erf}(\kappa r_{ia,ib})}{4\pi\epsilon_0 r_{ia,ib}} \\ & + \sum_{i=1}^{N}\sum_{a=1}^{3}[\chi_a q_{ia} + 0.5\sum_{b=1}^{3} q_{ia}q_{ib}J_{ab}(r_{ia,ib})] - Nu_{\text{gp}} \end{aligned} \quad (13)$$

where ϵ and σ are the Lennard−Jones parameters; $r_{\text{iO},j\text{O}}$ is the oxygen−oxygen distance between molecule i and j; $c(r_{\text{iO},j\text{O}})$ is equal to 1 when $r_{\text{iO},j\text{O}} \leq r_{\text{cut}}$ (the spherical potential truncation for Lennard−Jones interactions), or 0 otherwise; and $E_{\text{tail-LJ}}$ is the usual analytical tail correction for the Lennard−Jones potential.[16] The variables V, ϵ_0, q_{ia} are the volume of the simulation box, the permittivity of vacuum, and the fluctuating charge on site a of molecule i. κ, erf(x), and erfc(x) are the Ewald screening parameter, and the error and complementary error functions, respectively. $\mathbf{k}$ is the reciprocal lattice vector of the periodic system defined by $\mathbf{k} = 2\pi(\mathbf{h}^{-1})^t(l\ m\ n)$, where $\mathbf{h}$ is the matrix of basis vectors of the simulation box, l,m,n are integers. $K_{\max}$ denotes the upper bound of the reciprocal space summation, that is $l^2 + m^2 + n^2 \leq K_{\max}^2$. χ and J are parameters determined from the ionization potential and the electron affinity and are dependent on the atom type, and u_{gp} is the gas-phase energy of an individual molecule.

As discussed in section 2.C, the ANES-MC calculations can be performed using a constraint on the neutrality of every molecule,

$$\sum_{a=1}^{3} q_{i,a} = 0 \qquad \text{for all } i \quad (14)$$

or a constraint on the neutrality of an entire phase,

$$\sum_{i=1}^{N}\sum_{a=1}^{3} q_{i,a} = 0 \quad (15)$$

where N is the number of water molecules in the phase (simulation box) of interest. This latter constraint allows for intermolecular charge transfer.

We have used the following potential truncations in our work (i) for canonical and Gibbs ensemble simulations with $N = 100$ or $N = 120$: $r_{cut} = 7.2$ Å, and (ii) for canonical and Gibbs ensemble simulations with $N = 500$: $r_{cut} = 10.5$ Å. The Ewald parameters for all simulations are $\kappa \times L = 5$ and $K_{max} = 5$.

3. Results and Discussion

A. Vapor−Liquid Coexistence Curves. Gibbs ensemble simulations were performed for systems containing 120 water molecules using the SPC−FQ, SPC−FQ with charge transfer, and TIP4P−FQ force fields, and for 500-molecule systems using the SPC/E and SPC−FQ force fields. In most cases, simulations were performed at four temperatures: 373, 423, 473, and 523 K. For the simulations of the 120-molecule SPC−FQ systems, the MM-MC method and the ANES-MC algorithm with $T_{elec} = 5$ K or $T_{elec} = \infty$ K were used. For all MM-MC simulations, more than 20 000 MC cycles (N MC moves per cycle) were used to equilibrate the systems, and production periods consisted of an additional 10^5 MC cycles. Simulations using the ANES-MC algorithm were usually initiated from the corresponding MM-MC simulation, equilibrated for 10^5 MC cycles (N MC moves per cycle not counting any electronic moves), and an additional 40 000 MC cycles were performed for the production periods. The 500-molecule simulations were performed using ANES-MC with $T_{elec} = 5$ K, and the equilibration and production periods each consisted of 20 000 MC cycles. In the MM-MC and ANES-MC with $T_{elec} = \infty$ K simulations, the maximum translational, rotational, and volume displacements were adjusted to yield acceptance rates close to 50%. Whereas the ANES-MC simulations with $T_{elec} = 5$ K used the maximum displacements discussed in section 2.C. In all ANES-MC simulations with $T_{elec} = 5$ K, the maximum displacement for the electronic moves was set to $d_{elec} = 0.03$ e,[27] whereas a larger value of $d_{elec} = 0.2$ e was used for the simulations with $T_{elec} = \infty$ K. R_{elec} is set to 1 for the ANES-MC simulations with $T_{elec} = \infty$ K, whereas for the ANES-MC simulations with $T_{elec} = 5$ K, two different values were chosen for R_{elec}, 1 or 10, to study its influence on the outcome of the Gibbs ensemble simulations.

All the Gibbs ensemble simulation results, including the vapor pressures, saturated vapor- and liquid-phase densities, averaged vapor and liquid-phase internal energies, heats of vaporizations, and averaged vapor- and liquid-phase dipole moments, are listed in Table 1. As mentioned before in the canonical ensemble simulations with ANES-MC algorithm, $R_{elec} = 1$ is sufficient for translational and rotational moves for both system sizes of $N = 100$ and $N = 500$, despite that there is a more dramatic deviation in the distribution of the electronic energy from the equilibrated one (given by the uncoupled harmonic oscillators) using $R_{elec} = 1$ than $R_{elec} = 10$, shown in Figure 1. In the Gibbs ensemble simulations for the SPC−FQ model with $N = 120$ and $T_{elec} = 5$ K, good agreement with the MM-MC calculations, which rigorously sample according to the BO limit, is also found in the ANES-MC simulations with $R_{elec} = 1$. However, in the simulations for the SPC−FQ model with $N = 500$ and simulations for the TIP4P−FQ model (both using $T_{elec} = 5$ K), the vapor densities were overestimated using $R_{elec} = 1$. This might be because (i) the offset in electronic energy from the equilibrated distribution is much bigger for $R_{elec} = 1$ than $R_{elec} = 10$ (see Figure 1); (ii) the offset might be system-size- and model-dependent; (iii) the offset causes a long tail in EMseq in the swap move (see Figure 6) and this long tail might be different for removal/insertion of a molecule from/into the liquid phase. However, using $R_{elec} = 10$ the results for the SPC−FQ model for both system sizes are consistent with those obtained from the MM-MC simulations (see Table 1). Treating the fluctuating charges as additional degrees of freedom with ANES-

TABLE 1: Numerical Results of the Gibbs Ensemble Monte Carlo Simulations for the SPC/E, SPC-FQ, and TIP4P-FQ Force Fields[a]

T	P	ρ_{vap}	ρ_{liq}	U_{vap}	U_{liq}	ΔH_{vap}	μ_{vap}	μ_{liq}
SPC/E (N = 500)								
373	43	0.00024	0.945	−0.03	−42.5	45.7	2.35	2.35
423	220	0.0012	0.897	−0.54	−39.6	42.3	2.35	2.35
473	830	0.0040	0.833	−2.6	−36.5	37.6	2.35	2.35
523	2400	0.014	0.757	−4.9	−33.5	31.7	2.35	2.35
573	5600	0.028	0.621	−7.9	−29.6	25.1	2.35	2.35
SPC-FQ (MM-MC: $N = 120$)								
373	590	0.0033	0.910	−0.4	−34.1	37.1	1.88	2.59
423	2100	0.012	0.827	−1.2	−29.8	31.6	1.89	2.46
473	5700	0.033	0.737	−3.5	−25.7	25.5	1.91	2.37
523	13200	0.111	0.580	−6.3	−20.4	16.1	1.97	2.24
SPC-FQ (ANES-MC: $N = 120$, $T_{elec} = 5$ K, $R_{elec} = 10$)								
423	1800	0.0010	0.826	−0.9	−29.9	32.2	1.88	2.47
473	6500	0.0041	0.741	−2.9	−25.8	25.7	1.92	2.35
523	13900	0.098	0.556	−5.8	−19.7	16.2	1.95	2.26
SPC-FQ (ANES-MC: $N = 120$, $T_{elec} = 5$ K, $R_{elec} = 1$)								
373	640	0.0039	0.906	−0.5	−34.2	36.6	1.88	2.59
423	2500	0.015	0.835	−1.4	−30.0	31.5	1.88	2.47
473	6900	0.044	0.731	−3.2	−25.5	25.2	1.93	2.37
523	13700	0.103	0.596	−5.7	−20.0	16.0	1.97	2.25
SPC-FQ (ANES-MC: $N = 500$, $T_{elec} = 5$ K, $R_{elec} = 10$)								
373	680	0.0042	0.928	−0.8	−34.8	36.9	1.88	2.61
423	2300	0.014	0.840	−1.4	−30.0	31.8	1.89	2.47
473	6900	0.052	0.734	−5.1	−25.7	23.0	1.97	2.35
523	13000	0.103	0.576	−5.7	−20.0	16.6	2.00	2.25
SPC-FQ (ANES-MC: $N = 500$, $T_{elec} = 5$ K, $R_{elec} = 1$)								
373	940	0.006	0.911	−0.5	−34.2	36.6	1.88	2.59
423	3300	0.020	0.830	−1.9	−30.0	30.9	1.90	2.48
473	9600	0.068	0.737	−4.5	−25.7	23.5	1.95	2.37
523	15000	0.107	0.493	−6.0	−18.0	14.4	1.98	2.21
SPC-FQ (ANES-MC: $N = 120$, $T_{elec} = \infty$ K, $R_{elec} = 1$)								
373	430	0.0026	0.913	2.8	−31.3	37.0	1.90	2.62
423	2000	0.011	0.834	2.4	−26.5	32.0	1.92	2.50
473	5500	0.032	0.736	1.4	−21.8	26.2	1.95	2.41
523	13200	0.091	0.543	−1.1	−15.0	16.1	2.01	2.27
SPC-FQ with charge transfer (MM-MC: $N = 120$)								
373	360	0.0022	0.906	−1.0	−34.8	36.7		
423	1400	0.010	0.825	−2.4	−30.7	30.8		
473	4000	0.028	0.719	−3.9	−26.4	24.9		
523	10700	0.096	0.591	−8.3	−21.8	15.2		
TIP4P-FQ (ANES-MC: $N = 120$, $T_{elec} = 5$ K, $R_{elec} = 1$)								
373	1200	0.008	0.922	−1.2	−34.7	36.2	1.88	2.46
423	4400	0.032	0.866	−3.1	−30.9	30.0	1.91	2.36
473	8100	0.057	0.749	−4.0	−26.2	24.9	1.95	2.29
TIP4P-FQ (ANES-MC: $N = 120$, $T_{elec} = 5$ K, $R_{elec} = 10$)								
373	390	0.0024	0.932	−0.5	−34.5	36.9	1.86	2.45
423	1800	0.011	0.872	−1.2	−31.2	33.1	1.88	2.38
473	6300	0.039	0.796	−3.5	−27.5	26.7	1.92	2.31
TIP4P-FQ (ANES-MC: $N = 120$, $T_{elec} = \infty$ K, $R_{elec} = 1$)								
323	55	0.00037	0.988	2.6	−36.3	41.5	1.89	2.58
373	370	0.0022	0.935	2.8	−31.8	37.6	1.91	2.49
423	1600	0.0093	0.869	2.4	−27.5	32.9	1.92	2.41
473	5200	0.032	0.784	0.6	−23.3	26.7	1.95	2.34
523	11500	0.088	0.655	−2.1	−18.4	18.3	2.00	2.26

[a] Temperatures, saturated vapor pressures, saturated vapor- and liquid-phase densities, average vapor and liquid-phase internal energies, heats of vaporization, and average vapor- and liquid-phase dipole moments are given in units of K, kPa, g/mL, kJ/mol, and Debye, respectively.

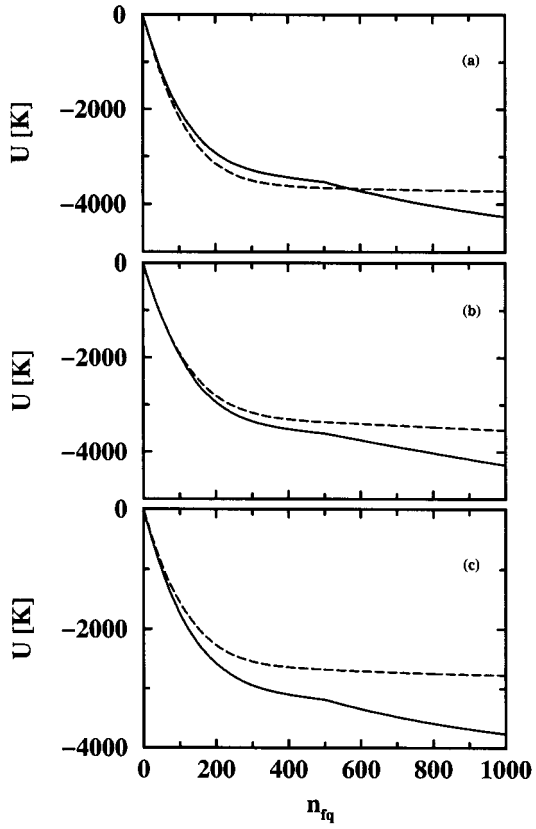

Figure 6. The mean evolution of the total energy (liquid and vapor phases) averaged over a period of 10^3 swap moves versus the number of electronic moves during the EMseq of an ANES-MC particle swap move (first 500 moves for the preferential selection of the sites for the electronic move followed by 500 moves on the randomly chosen sites) starting from a final configuration in the Gibbs ensemble simulation using $R_{elec} = 1$ (solid lines) or $R_{elec} = 10$ (dashed lines) for (a) 120-molecule system for the SPC−FQ model, (b) 500-molecule system for the SPC−FQ model, and (c) 120-molecule system for the TIP4P−FQ model.

MC does recover the correct distributions for the nuclear properties. Furthermore, even a choice of $T_{elec} = \infty$ K works for force fields with quadratic coupling of the electronic degrees of freedom. Here it should be emphasized that the total energies increase for ANES-MC simulations with $T_{elec} = 5$ K or ∞ K because heat is pumped into the electronic degrees of freedom (see Table 1). However, this happens for all molecules in both phases and the heats of vaporization are therefore not influenced by the changes in electronic energies (see Table 1).

Figure 7 shows a comparison of the vapor−liquid coexistence curves for the TIP4P−FQ model obtained by different simulation methods. As described in the Introduction, Medeiros and Costas[23] used a pseudo-Gibbs ensemble formalism and performed only partial minimization of the electronic structure during their Monte Carlo simulations. Yezdimer and Cummings[24] performed a Gibbs−Duhem integration[25] using the $T = 298$ K coexistence point determined by Medeiros and Costas as the initial reference point. Good agreement between the different simulation studies is found for the saturated liquid densities and also for other liquid-phase properties (e.g. for internal energy and average molecular dipole moments, see Table 1 of this article and Table 1 of ref 24). However, significant deviations between the Yezdimer and Cummings' results and our ANES-MC calculations are evident for the saturated vapor densities (and vapor pressures, see Table 1). As an additional test, independent ANES-MC calculations ($T_{elec} = \infty$, $R_{elec} = 1$) in the grand canonical ensemble[33] (using a

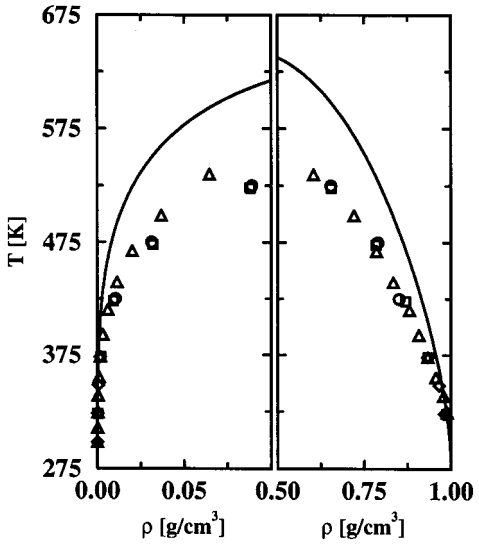

Figure 7. Comparison of the vapor−liquid coexistence curves calculated for the TIP4P−FQ force field using ANES-MC Gibbs ensemble simulations ($T_{elec} = \infty$ K, $R_{elec} = 1$, squares), ANES-MC grand canonical simulations ($T_{elec} = \infty$ K, $R_{elec} = 1$, circles), pseudo-Gibbs ensemble simulations by Mederios and Costas (diamonds),[23] and Gibbs−Duhem integration by Yezdimer and Cummings (triangles).[24] Experimental coexistence data are shown as solid lines.[52]

simulation box length of 20 Å) were performed. Histogram-reweighting techniques[34−38] were used to obtain the coexistence curve in the near-critical region from these simulations, and agreement with our GEMC calculations is very satisfactory for both vapor and liquid phases (see Figure 7). Our results suggest that the pseudo-Gibbs ensemble approach in conjunction with the partial optimization of the electronic structure results in a systematic bias that lowers the vapor density. This also accounts for the discrepancies between our work and the calculations of Yezdimer and Cummings. Because the Gibbs−Duhem integration is not "self-correcting",[25] starting from an initial condition biased to a lower vapor density will result in a systematic underprediction of the vapor density across the entire temperature range.

Figure 8 shows a comparison of the coexistence curves for the different water force fields investigated here. The most important result is that the SPC−FQ and TIP4P−FQ force fields do not yield a satisfactory description of vapor−liquid phase equilibria. In particular, the critical temperatures are largely underestimated. From extrapolation of our GEMC simulation results,[20] we can estimate critical temperatures of about 540 and 570 K for the SPC−FQ and TIP4P−FQ force fields, and the corresponding critical densities are close to 0.33 and 0.35 g/mL, respectively. However, these estimates of the critical properties should be viewed with caution because of the unique features of the vapor−liquid coexistence curve of water as observed experimentally (apparent flatness of the near-critical region and deviations from the law of rectilinear diameters[17,40]). A mixed-field analysis[38,39] of the results obtained from the ANES-MC simulations in the grand canonical ensemble yields $T_c = 558.9$ K and $\rho_c = 0.307$ g/mL (for a simulation box length of 30 Å). For comparison, the experimental critical data are $T_c = 647$ K and $\rho_c = 0.317$ g/mL. The corresponding values for the SPC/E force field obtained from our Gibbs ensemble calculations are 626 K and 0.29 g/mL, which are in good agreement with previous simulation estimates for the SPC/E force field.[41−44]

In addition, MM-MC calculations in the Gibbs ensemble were carried out for the SPC−FQ force field using a constraint on

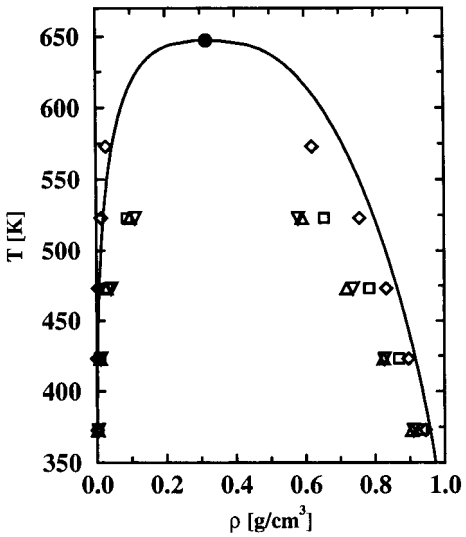

Figure 8. Comparison of the vapor−liquid coexistence curves calculated for the SPC/E (diamonds), SPC−FQ without charge transfer (MM-MC, triangle down), SPC−FQ with charge transfer (MM-MC, triangle up), and TIP4P−FQ (ANES-MC/GEMC with $T_{elec} = \infty$ K and $R_{elec} = 1$, squares) force fields. Experimental coexistence data and critical point are shown as solid lines and filled circle, respectively.[52]

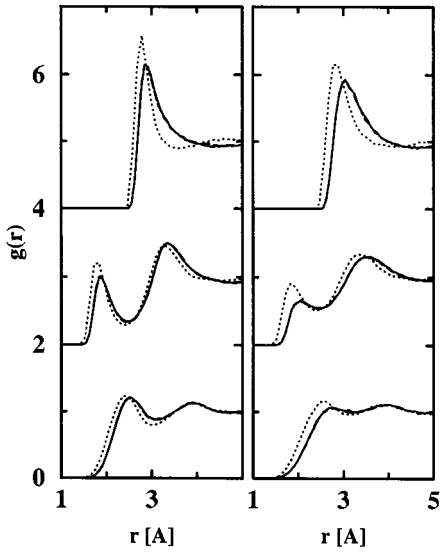

Figure 9. Oxygen−oxygen (top, vertically offset by 4 units), oxygen−hydrogen (middle, vertically offset by 2 units), and hydrogen−hydrogen (bottom) radial distribution functions for the vapor phase of SPC/E water (dotted lines), SPC−FQ water sampled with the ANES-MC algorithm ($T_{elec} = 5$ K, $R_{elec} = 10$, dashed line), and with the MM-MC algorithm (solid lines) at $T = 373$ K (left column) and at $T = 573$ K for SPC/E and $T = 523$ K for SPC−FQ (right column).

the neutrality of each phase.[45] Maybe somewhat surprisingly, allowing for intermolecular charge transfer does not result in a significant change of the coexistence curve for the SPC−FQ model (see Figure 8 and Table 1), despite the presence of (partial) ions.

The saturated vapor pressures and heats of vaporization of all the different sets of simulations are listed in Table 1. The saturated vapor pressures calculated for the SPC/E model are consistently too low, whereas those for the SPC−FQ model are too high. The low vapor pressures of the SPC/E model are consistent with too high heats of vaporization (5 kJ/mol too high at 373 K, but closer to the experimental results near the critical point). On the contrary, the SPC−FQ model yields a heat of vaporization closer to the experimental result at 373K, but differs by 14 kJ/mol at 523 K. That is, for both models the heats of vaporization change too rapidly with increasing temperature compared with the experimental data.

The features exhibited by both SPC−FQ and TIP4P−FQ models, such as too low critical temperatures, and too low heats of vaporizations and too high vapor pressures at higher temperatures were also found by Kiyohara et al.[11] for the dipole-polarizable TIP4P/P, SPC/P, and SCPDP models. The critical temperatures for these models were 587, 551, and 538 K, respectively (compared with 558.9 K for the TIP4P−FQ model, 540 K for the SPC−FQ model, 626 K for the SPC/E model, and 647 K for the experimental result). To improve the performance of these dipole-polarizable force fields, Kiyohara et al. attempted to optimize the parameters for the Lennard−Jones (LJ) site on the oxygen atom. They found that very small changes in these parameters can result in dramatic changes in the location of the critical point, the saturated densities, and liquid structures, pointing to the importance of the short-range repulsive part of the LJ interactions. However, Kiyohara et al. concluded that solely adjusting the LJ parameters was not sufficient to make any of the dipole-polarizable water models suitable for phase equilibrium calculations. It should be noted that although the TIP4P/P and SPC/P force fields make use of the same Lennard−Jones parameters as the parent fixed-charge force fields, different sets of Lennard−Jones parameters were fitted by Rick et al.[5] for the TIP4P−FQ and SPC−FQ force fields.

B. Radial Distribution Functions and Charge Distributions. RDFs calculated for the liquid phases of the SPC/E and SPC−FQ force fields along the saturation line are compared in Figure 9 for $T = 373$ K (both models), 573 K (SPC/E), and 523 K (SPC−FQ). Results for the SPC−FQ model were obtained using the MM-MC and ANES-MC (with $T_{elec} = 5$ K) algorithms. Increasing the temperature results in major disturbances of the hydrogen-bonded network structure, as is evident from reduced heights of the first peaks in the O−O, O−H, and H−H RDFs and the disappearance of the pronounced first minimum in the O−H RDFs. It is noteworthy that the SPC/E model yields a more ordered structure at $T = 573$ K than the SPC−FQ model at 523 K. This is consistent with the report[46] that the SPC/E model overestimates the hydrogen-bonded structure at high temperature, partly because of its lack of adaptability of the dipole moment to the lower-density environment. It should be noted that the RDFs calculated for the SPC−FQ model with ANES-MC agree very well with those obtained by MM-MC, that is the distributions of nuclear positions are apparently sampled from the limiting BO distribution using the ANES-MC algorithm.

Figure 10 shows the evolution of the charge distributions observed for the oxygen and hydrogen sites of the SPC−FQ model (similar changes are also found for the TIP4P−FQ model), and Figure 11 depicts the corresponding changes in the dipole moment (also for the TIP4P−FQ model). In the liquid phase, the average dipole moment for the SPC−FQ model decreases from around 2.60 D at $T = 373$ K to 2.25 D at $T = 523$ K (see also Table 1), whereas the widths of the distributions become progressively narrower at high temperatures. This change in the charge distributions is caused by a decrease in liquid-phase density and a decrease in the local heterogeneity. In contrast, the average dipole moments of vapor-phase molecules change to a lesser extent (from 1.9 D at $T = 373$ K to 2.0 D at $T = 523$ K). However, the increased widths and the tailing to larger charges found for the vapor phase at the higher

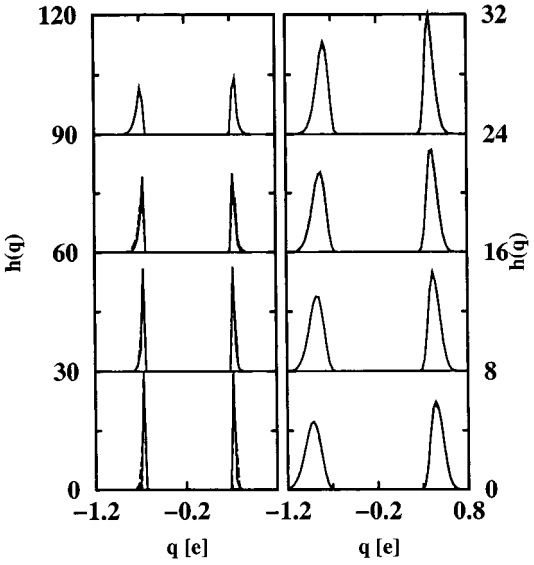

Figure 10. Oxygen and hydrogen charge distributions in the vapor (left column) and liquid (right column) phases obtained for the SPC−FQ force field using ANES-MC ($T_{elec} = 5$ K, $R_{elec} = 10$, dashed lines) and MM-MC (solid lines) at $T = 523$, 473, 423, and 373 K (vapor phase: vertically offset by 90, 60, 30, and 0 units, respectively; liquid phase: vertically offset by 24, 16, 8, and 0 units, respectively).

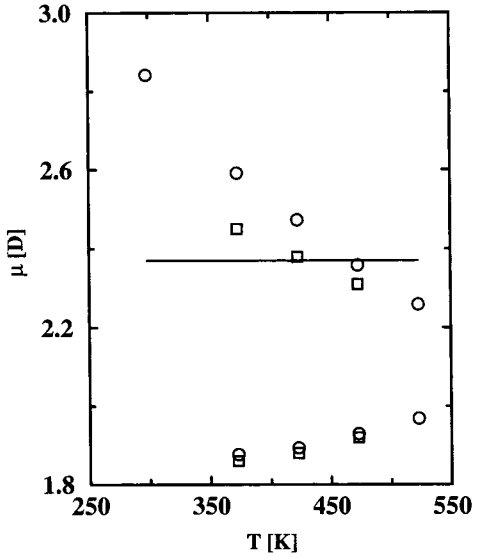

Figure 11. Vapor- and liquid-phase dipole moments as function of temperature calculated for the SPC−FQ (circles) and TIP4P−FQ (squares) force fields. The fixed dipole moment of the SPC/E model is shown as a solid line for comparison.

temperatures is evidence for increased formation of small water clusters (mostly dimers). Again, results obtained with the ANES-MC algorithm ($T_{elec} = 5$ K) agree rather well with those calculated using MM-MC (see also dipole moments listed in Table 1 for the other ANES-MC simulations). The small differences observed in the vapor phases can be attributed to the thermal broadening caused by introducing the fictitious electronic degrees of freedom, whereas in the liquid phase, the thermal broadening appears negligible compared with the broadening caused by the heterogeneity of liquid environment.

The distributions of molecular charges at different temperatures calculated for the SPC−FQ model with constraints on the neutrality of each phase are plotted in Figure 12. In the liquid phase, (partial) ions with charges of up to 0.2 e in magnitude are observed, but 80% of the molecular charges are smaller than 0.1 e in magnitude. There is relatively little change

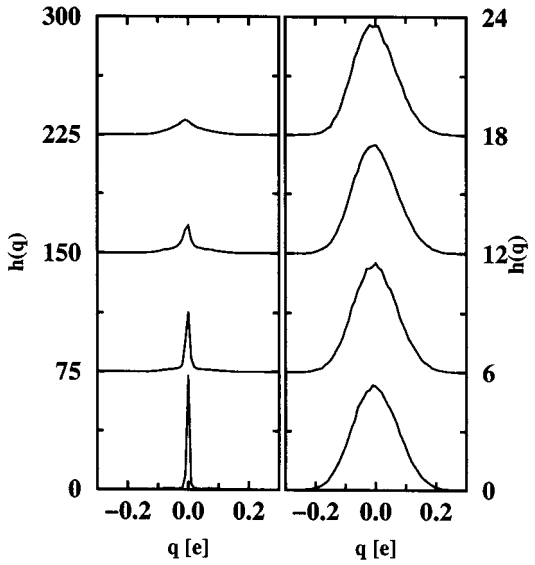

Figure 12. Molecular charge distributions in the vapor (left column) and liquid (right column) phases obtained for the SPC−FQ force field with intermolecular charge transfer at $T = 523$, 473, 423, and 373 K (vapor phase: vertically offset by 225, 150, 75, and 0 units, respectively; liquid phase: vertically offset by 18, 12, 6, and 0 units, respectively).

in the liquid-phase molecular charge distributions across the range of temperature studied here, and the charge distribution obtained from a canonical simulation at $T = 298$ K and $\rho = 1.0$ g/mL is very similar to that shown for the liquid phase at $T = 373$ K. There is considerably more temperature dependence in the vapor-phase molecular charge distribution. At the lower temperatures, most vapor-phase molecules are isolated and are not charged. However, at the higher temperatures some clusters are formed in the vapor phase and charge transfer occurs. At $T = 373$ K, we can observe three distinct peaks: the main peak centered at a molecular charge of 0.0 e and two symmetric side peaks at ± 0.07 e which can be attributed to dimer formation. The maximum extent of charge transfer in the vapor phase (at $T = 373$ K) is similar to the value of 0.12 e observed for the minimum energy dimer of this model.

As mentioned above, allowing for intermolecular charge transfer in the SPC−FQ model does not seem to alter the vapor−liquid coexistence curves, despite the presence of (partial) ions. Therefore we have also performed an additional ANES-MC simulation in the canonical ensemble ($T = 298$ K and $\rho = 1.0$ g/mL) for the SPC−FQ model constraining the neutrality of the entire system. The average internal energy changes by only 0.7 kJ/mol (−42.05 kJ/mol and −41.33 kJ/mol with and without charge transfer, respectively). Even more surprising is the small effect on the RDFs (shown in Figure 13). Allowing for charge transfer leads only to a barely noticeable shift to smaller distances for the first peaks of the O−O and O−H RDFs. Charge transfer does not appear to lead to a substantial shortening of the hydrogen bonds. This might be a feature specific to the SPC−FQ model (or other similar models) for which the usual hydrogen-bonded O−O separation is already well within the (very steep) repulsive region of the Lennard−Jones potential.

D. Dielectric Constant. The dielectric constant was evaluated for the SPC/E and SPC−FQ (without and with intermolecular charge transfer) force fields for liquid water at $T = 298$ K and $\rho = 1.0$ g/mL using regular MC (for SPC/E) or ANES-MC and MM-MC (for SPC−FQ) simulations in the canonical ensemble. The dielectric constant can be calculated by the following fluctuation formula under the proper Ewald boundary condition[47]:

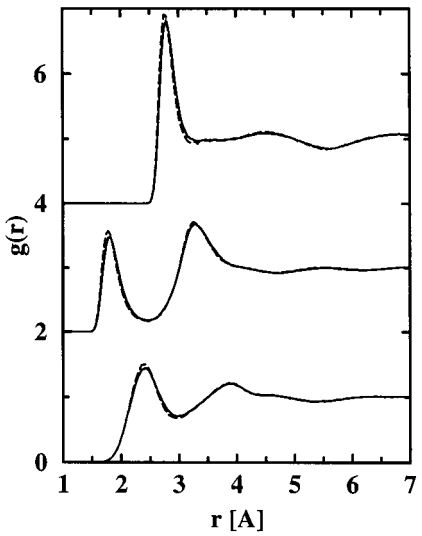

Figure 13. Oxygen−oxygen (top, vertically offset by 4 units), oxygen−hydrogen (middle, vertically offset by 2 units), and hydrogen−hydrogen (bottom) radial distribution functions for liquid water at $T = 298$ K and $\rho = 1.0$ g/mL for the SPC−FQ force field without charge transfer (solid line) and with charge transfer (dashed line).

$$\epsilon - 1 = \frac{4\pi\beta}{3V}(\langle \mathbf{M}^2\rangle - \langle \mathbf{M}\rangle^2) + \epsilon_\infty - 1 \qquad (14)$$

where $\mathbf{M}$ and V are the total dipole moment and volume of the simulation cell, respectively. $\beta = (k_B T)^{-1}$ is the inverse temperature, and ϵ_∞ is the high-frequency dielectric constant. For nonpolarizable models $\epsilon_\infty = 1$, whereas it has been reported to be 1.606 for the SPC−FQ model.[5] The convergence of the dielectric constant was monitored by plotting $\langle \mathbf{M}_x\rangle^2$, $\langle \mathbf{M}_y\rangle^2$, and $\langle \mathbf{M}_z\rangle^2$ against the length of each simulation. It was found that a (total) simulation length in excess of 10^6 MC cycles (N moves per cycles not counting any electronic moves) is required to obtain a precise determination of the dielectric constant (see Figure 14). As consistency check, we have performed multiple independent simulations for some systems. Using one long calculation of 4×10^6 MC cycles the dielectric constant for a 500-molecule system using the SPC/E model was calculated as 67 ± 2 in good agreement with other reports (70 ± 10,[48] 67 ± 10,[49] and 66 ± 13[50]).

The dielectric constant for the SPC−FQ model with a constraint on molecular neutrality was obtained by four different means. First, for a 100-molecule system, five independent ANES-MC simulations ($T_{elec} = 5$ K, $R_{elec} = 1$, $d_{trans} = 0.1$ Å, and $d_{rot} = 0.1$ rad) of 5×10^6 MC cycles (each) were performed and yielded a dielectric constant of 114 ± 6 in good agreement with the value obtained by Rick et al.[5] using the molecular dynamics technique. The average of the five simulations is plotted in Figure 14. Second, a 500-molecule system was used for additional ANES-MC calculations (with the same set of simulation parameters as for the first set of simulations); again five independent simulations were used, but the length of each simulation was only 6×10^5 MC cycles. The dielectric constant for the 500-molecule system is 117 ± 30. Third, an additional set of five simulations was performed using the (much more expensive) MM-MC algorithm on a 100-molecule system (with $d_{trans} = 0.3$ Å and $d_{rot} = 0.4$ rad). In this case, the length of each simulation was only 3×10^5 MC cycles (but the maximum displacements are larger) and the resulting dielectric constant is 113 ± 17. It is evident that there is little effect caused by either the system size or by the different MC algorithms. Fourth, to evaluate the influence of the adiabatic separation on the dielectric constant obtained for this type of force field, we have also performed one long simulation (5×10^6 MC cycles) for a 100-molecule system using ANES-MC and $T_{elec} = \infty$ K ($R_{elec} = 1$, $d_{trans} = 0.3$ Å, and $d_{rot} = 0.4$ rad). The results are also plotted in Figure 14, and the calculated dielectric constant is 119 ± 10. Thus the additional thermal fluctuations in the charge distributions of individual atomic sites (see Figure 4) do not result in a significant change of the dielectric constant. The internal energies (including the electronic contribution) averaged over these very long simulations are -41.48 ± 0.05 kJ/mol, -41.25 ± 0.04 kJ/mol, -41.33 ± 0.05 kJ/mol, and -38.82 ± 0.03 kJ/mol (in the same order as described above). The heat capacity of the fictitious electronic degrees of freedom is solely responsible for the differences between MM-MC, ANES-MC ($T_{elec} = 5$ K), and ANES-MC ($T_{elec} = \infty$ K). Both the estimates of the dielectric constant and of the internal energy agree well with the corresponding results of molecular dynamics calculations (118 and −41.4 kJ/mol).[5]

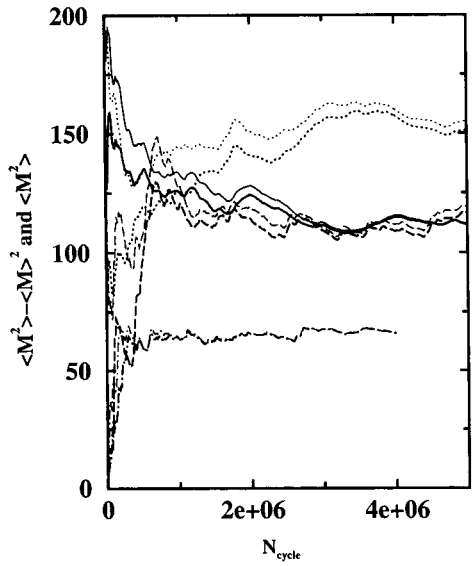

Figure 14. Running averages of $(4\pi\beta/3V)[\langle \mathbf{M}^2\rangle - \langle \mathbf{M}\rangle^2]$ (thick lines) and $(4\pi\beta/3V)\langle \mathbf{M}^2\rangle$ (thin lines) used in the calculations of the dielectric constants. Solid, dashed, dotted, and dashed−dotted lines represent the results obtained for SPC−FQ without charge transfer using $T_{elec} = 5$ K, for SPC−FQ without charge transfer using $T_{elec} = \infty$ K, for SPC−FQ with charge transfer with $T_{elec} = 5$ K, and for SPC/E, respectively.

Finally, a single ANES-MC simulation of 5×10^6 cycles was performed for a 100-molecule systems using the SPC−FQ model with a constraint on the neutrality of the entire system. The resulting dielectric constant is 153 ± 8 (see Figure 14), which is 30% larger than observed for the SPC−FQ model without charge transfer. Thus, although charge transfer had little influence on the internal energy, the RDFs, or the coexistence curve, relaxing the constraint of molecular neutrality does alter the dielectric constant. Currently, we are not able to judge whether these dual-level effects are peculiar to the SPC−FQ model or are more general for other polarizable models.

IV. Conclusions

The validity and efficiency of the ANES-MC algorithm have been investigated for simulations in the Gibbs ensemble. The theoretical analysis provided previously[27] allows us to derive the acceptance rules for the volume-exchange and particle-swap moves needed in Gibbs ensemble simulations (and applicable

with obvious modifications to volume moves in isobaric−isothermal ensemble simulations and particle deletions/insertions in grand canonical ensemble simulations). The ANES-MC method requires a compromise between rigor (the adiabatic limit is rigorously approached as $T_{elec} \rightarrow 0$ K and as $R_{elec} \rightarrow \infty$) and computational efficiency that can be obtained with a judicious choice of ANES-MC parameters (e.g., $T_{elec} = 5$ K, $R_{elec} = 10$, and suitable sets of maximum nuclear displacements). In particular, for polarizable force fields that involve quadratic coupling of the electronic degrees of freedom the ANES-MC algorithm offers a very efficient route for MC simulations in all statistical-mechanical ensembles. The particle swap move requires an additional preferential selection of the electronic degrees of freedom, for which moves are attempted, to achieve efficient sampling. From comparison of various thermodynamic and structural properties, it is evident that results in close agreement with the MM-MC method (which rigorously samples from the BO limit) can be obtained. More importantly, the computational cost of the ANES-MC algorithm scales as N^2 with increases in system size (assuming that no additional techniques, such as a neighbor list, are used), whereas conventional iterative schemes scale as N^3, and the N^4 scaling of the MM-MC algorithm is prohibitive for most systems.

The vapor−liquid-phase equilibrium properties of the SPC−FQ and TIP4P−FQ force fields proposed by Rick et al.[5] do not show an improvement over the fixed-charge SPC/E force field. In particular, although the SPC−FQ and TIP4P−FQ models yield satisfactory heats of vaporization at low temperature, these quantities change too rapidly with increasing temperature, and result in far too low estimates for the critical temperature. A forthcoming publication will demonstrate that this deficiency can be removed by introducing a coupling of the Lennard−Jones parameters to the fluctuating charge on the oxygen atomic site.[51] Allowing for intermolecular charge transfer in the SPC−FQ model does not lead to significant changes in internal energy, molecular structure, or coexistence curve, but results in an increase of the dielectric constant by 30% at 298 K.

Acknowledgment. We would like to thank Glenn Martyna, Mark Tuckerman, Woods Halley, Donald Truhlar, and Darrin York for many stimulating discussions. Financial support from the National Science Foundation (CTS-9813601), a Camille and Henry Dreyfus New Faculty Award, a McKnight/Land-Grant Fellowship, an Alfred P. Sloan Research Fellowship, a Stanwood Johnston Memorial Fellowship (B.C.), and a Departmental Dissertation Fellowship (B.C.) is gratefully acknowledged. Part of the computer resources were provided by the Minnesota Supercomputing Institute.

References and Notes

(1) Sprik, M.; Klein, M. L. *J. Chem. Phys*. **1988**, *89*, 7556.
(2) Ahlström, P.; Wallqvist, A.; Engström, S.; Jönsson, B. *Mol. Phys*. **1989**, *68*, 563.
(3) Cieplak, P.; Kollman, P.; Lybrand, T. *J. Chem. Phys*. **1992**, *97*, 13841.
(4) Wallqvist, A.; Berne, B. J. *J. Phys. Chem.* **1993**, *97*, 13841.
(5) Rick, S. W.; Stuart, S. J.; Berne, B. J. *J. Chem. Phys*. **1994**, *101*, 6141.
(6) Chialvo, A. A.; Cummings, P. T. *J. Chem. Phys*. **1996**, *105*, 8274.
(7) Svishchev, I. M.; Kusalick, P. G.; Wang, J.; Boyd, R. J. *J. Chem. Phys*. **1996**, *105*, 4742.
(8) Laasonen, K.; Sprik, M.; Parrinello, M. *Chem. Phys. Lett*. **1993**, *99*, 9080.
(9) Sprik, M.; Hutter, J.; Parrinello, M. *J. Chem. Phys*. **1996**, *105*, 1142.
(10) Gao, J. *J. Chem. Phys*. **1998**, *109*, 2346.
(11) Kiyohara, K.; Gubbins K. E.; Panagiotopoulos, A. Z. *Mol. Phys*. **1998**, *94*, 803.
(12) Berendsen, H. J. C.; Postma, J. P. M.; von Gunsteren, W. F.; Hermans, J. *Intermolecular Forces*; Pullman, B., Ed.; Reidel: Dordrecht, 1981; p 331.
(13) Berendsen, H. J. C.; Grigera, J. R.; Straatsma, T. P. *J. Phys. Chem.* **1987**, *91*, 6269.
(14) Jorgensen, W. L.; Chandrasekhar, J.; Madura, J. D.; Impey, R. W.; Klein, M. L. *J. Chem. Phys.* **1983**, *79*, 926.
(15) Wallquist, A.; Mountain, R. D. *Rev. Comput. Chem*. **1999**, *13*, 183.
(16) Allen, M. P.; Tildesley, D. J. *Computer Simulation of Liquids*; Oxford University Press: Oxford, 1987.
(17) Frenkel, D.; Smit, B. *Understanding Molecular Simulation*; Academic Press: San Diego, 1996.
(18) Panagiotopoulos, A. Z. *Mol. Phys*. **1987**, *61*, 813.
(19) Panagiotopoulos, A. Z.; Quirke, N.; Stapleton, M.; Tildesley, D. *J. Mol. Phys.* **1988**, *63*, 527.
(20) Smit, B.; de Smedt, Ph.; Frenkel, D. *Mol. Phys*. **1989**, *68*, 931.
(21) de Pablo, J. J.; Prausnitz, J. M.; Strauch, H. J.; Cummings, P. T. *J. Chem. Phys*. **1990**, *93*, 7355.
(22) Strauch, H. J.; Cummings, P. T. *J. Chem. Phys*. **1992**, *96*, 864.
(23) Medeiros, M.; Costas, M. E. *J. Chem. Phys*. **1997**, *107*, 2012.
(24) Yezdimer, E. M.; Cummings, P. T. *Mol. Phys*. **1999**, *97*, 993.
(25) Kofke, D. A. *Adv. Chem. Phys*. **1999**, *105*, 405.
(26) Martin, M. G.; Chen, B.; Siepmann, J. I. *J. Chem. Phys*. **1998**, *108*, 3383.
(27) Chen, B.; Siepmann, J. I. *Theor. Chem. Acc*. **1999**, *103*, 87.
(28) Andersen, H. C. *J. Chem. Phys*. **1980**, *72*, 2384.
(29) Car, R.; Parrinello, M. *Phys. Rev. Lett*. **1985**, *55*, 2471.
(30) Saboungi, M.-L.; Rahman, A.; Halley, J. W.; Blander, M. *J. Chem. Phys*. **1988**, *88*, 5818.
(31) Wilson, M.; Madden, P. A. *J. Phys. Condens. Matter* **1993**, *5*, 2687.
(32) In cases where the coupling between electronic and nuclear degrees of freedom is not quadratic, the phase volume of the electronic partition depends on the set of nuclear coordinates. Thus the electronic and nuclear parts of the partition function cannot be separated in straightforward fashion. For these cases, adiabatic sampling of electronic and nuclear degrees of freedom in the BO limit is only achieved for $T_{elec} \rightarrow 0$ K and $R_{elec} \rightarrow \infty$.[27] Similar problems are encountered in Car−Parrinello molecular dynamics (Bornemann, F. A.; Schütte, C. *Numer. Math*. **1998**, *78*, 359).
(33) Potoff, J. J.; Chen, B.; Siepmann, J. I., manuscript in preparation.
(34) Ferrenberg, A. M.; Swendsen, R. H. *Phys. Rev. Lett*. **1988**, *61*, 2635.
(35) Ferrenberg, A. M.; Swendsen, R. H. *Phys. Rev. Lett*. **1989**, *63*, 1195.
(36) Swendsen, R. H. *Physica A* **1993**, *194*, 53.
(37) Errington, J. R.; Panagiotopoulos, A. Z. *J. Chem. Phys*. **1998**, *109*, 1093.
(38) Potoff, J. J.; Panagiotopoulos, A. Z. *J. Chem. Phys*. **1998**, *109*, 10914.
(39) Wilding, N. B. *Phys. Rev. E* **1995**, *52*, 602.
(40) Rowlinson, J. S. *Liquids and Liquids Mixtures*; Butterworth Scientific Publications: London, 1959; p 60.
(41) Guissani, Y.; Guillot, B. *J. Chem. Phys*. **1993**, *98*, 8221.
(42) Alejandre, J.; Tildesley, D. J.; Chapela, G. A. *J. Chem. Phys*. **1995**, *102*, 4574.
(43) Boulougouris, G. C.; Economou, J. G.; Theodorou, D. N. *J. Phys. Chem. B* **1998**, *102*, 1029.
(44) Errington, J. R.; Kiyohara, K.; Gubbins, K. E.; Panogiotopoulos, A. Z. *Fluid Phase Equilib*. **1998**, *150*, 33.
(45) In principle, ANES-MC can also be used for Gibbs ensemble simulations with a neutrality constraint on each phase. In this case, a swap move has to involve the transfer of a randomly selected molecule *and* the transfer of a counter charge randomly taken from the same phase.
(46) Dang, L. X. *J. Phys. Chem. B* **1998**, *102*, 620.
(47) Hansen, J. P.; McDonald, I. R. *Theory of Simple Liquids*, 2nd ed.; Academic Press: London, 1986.
(48) Watanabe, K.; Klein, M. L. *Chem. Phys*. **1989**, *131*, 157.
(49) Smith, D. E.; Dang, L. X. *J. Chem. Phys*. **1994**, *100*, 3757.
(50) Errington, J. R.; Panogiotopoulos, A. Z. *J. Phys. Chem. B* **1998**, *102*, 7470.
(51) Chen, B.; Xing, J.; Siepmann, J. I. *J. Phys. Chem. B* **2000**, *104*, 2391.
(52) NIST Chemistry WebBook, http://webbook.nist.gov/chemistry.